JACS
JOURNAL OF THE AMERICAN CHEMICAL SOCIETY
pubs.acs.org/JACS
Article

Structure and Catalytic Characterization of a Second Framework Al(IV) Site in Zeolite Catalysts Revealed by NMR at 35.2 T

Kuizhi Chen,* Sarah Horstmeier, Vy. T. Nguyen, Bin Wang, Steven P. Crossley, Tram Pham, Zhehong Gan, Ivan Hung, and Jeffery L. White*

Cite This: J. Am. Chem. Soc. 2020, 142, 7514−7523
Read Online
ACCESS | Metrics & More | Article Recommendations | Supporting Information

ABSTRACT: Ultrahigh field $^{27}Al\{^{1}H\}$ 2D correlation NMR experiments demonstrate that at least two framework Al(IV) sites with hydroxyl groups can exist in acidic zeolite catalysts in their dehydrated and catalytically active states. In addition to the known Al(IV) at the framework bridging acid site (BAS), a new site created by a second tetrahedral Al atom and its hydroxyl group protons in zeolite HZSM-5 is clearly resolved at 35.2 T field strengths, enabled by recently developed series-connected hybrid (SCH) magnet technology. Coupled with computational modeling, extensive ^{27}Al MQMAS experiments at multiple field strengths, and ^{1}H MAS NMR experiments, these data indicate that this second tetrahedrally coordinated Al site (denoted Al(IV)-2) experiences an increased chemical shift and unique quadrupolar parameters relative to the BAS in both dehydrated and hydrated states. These new experimental data, supported by computational and catalytic reaction work, indicate that the second site arises from partially bonded framework $(SiO)_{4-n}$-$Al(OH)_n$ species that significantly increase catalyst reactivity in benzene hydride-transfer and *n*-hexane cracking reactions. Al(IV)-2 sites result either from framework crystallization defects or from incomplete postsynthetic hydrolysis of a framework Al, prior to the formation of extraframework Al. Populations of this second acidic proton site created by the Al(IV)-2 species are shown to be controlled via postsynthetic catalyst treatments, should be general to different catalyst structures, and significantly enhance catalyst reactivity in the cited probe reactions when they are present. The results herein communicate the highest magnetic field strength data on active zeolite catalyst structures to date and enable for the first time the detection of Al and H association on a dry HZSM-5 catalyst, i.e., under conditions representative of typical end-use processes.

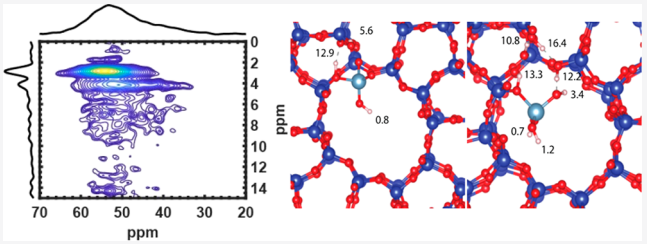

INTRODUCTION

The definition of the structure of an active site and its possible structural variations is a critical step in developing fundamental insights into catalyst function and exploiting those insights for improved catalytic materials.[1,2] Acidic zeolite catalysts have been successfully employed in several industrial processes,[3−5] most of which involve high-temperature conditions where water vapor or liquid water are absent. However, a growing interest exists in understanding the fate of zeolite acid sites in the presence of water, e.g., in catalytic transformation of feedstocks derived from alcohols and biomass,[6,7] which also requires accurate characterization of acid site structures both in the absence and presence of water. Tetrahedrally coordinated framework Al atoms in zeolites create Brønsted acid sites through the charge-balancing function of a proton, and while it is known that crystallographically inequivalent framework Al sites can exist, e.g., twelve sites in the MFI family of zeolites of which HZSM-5 catalysts are members, reports have demonstrated that the resulting bridging acid sites (BAS) in the different zeolite catalyst types are essentially identical in their ability to transfer a proton.[3] The MFI family of zeolite catalysts, most notably ZSM-5, is important to practical catalysis due to its efficacy in isomerization, alkylation, and disproportion reactions,[4,5,8] as well as in the conversion of methanol to hydrocarbons.[9,10] Currently, there is significant activity in literature devoted to determining if single active sites, multiple sites, or a distribution of active acid sites exist in this commercially and academically important catalyst.[11−15] Recent reports suggest that proximity of the BAS's with each other, and with extra-framework hydroxyl groups, leads to acid site heterogeneity in many HZSM-5 catalysts, particularly at high Al content.[16−20] Here, the recently developed series-connected hybrid (SCH) magnet at 35.2 T[21] is coupled with two-dimensional $^{27}Al\{^{1}H\}$ correlation techniques[22−24] to conclusively identify a second Al(IV) species and accompanying Brønsted proton site in dry HZSM-5 catalysts. This second site in HZSM-5, while structurally unique compared to its

Received: January 16, 2020
Published: April 1, 2020

https://dx.doi.org/10.1021/jacs.0c00590
J. Am. Chem. Soc. 2020, 142, 7514−7523

known BAS, is also characterized by four-coordinate Al and denoted here as Al(IV)-2. Detailed experiments and supporting computational investigations on both dry and partially hydrated HZSM-5 indicate that Al(IV)-2 is associated with a partially bonded framework species that generates a Brønsted site and similarly responds to postsynthetic treatments including solvent washing and hydrothermal exposure that have previously been used for modifying the distribution of extra-framework aluminum species. This new structure information is paramount to understanding the function of HZSM-5 catalysts in dry operating conditions as well as predicting the impact of water and other postsynthetic procedures on catalyst function, all of which are important to extending zeolite catalysts to increasingly complex feedstocks. We propose that the new acid site information reported here clarifies recent literature detailing the fact that catalysts with highest activity appear to have species other than isolated framework BAS's,[12−15] addresses uncertainties surrounding increased activity for some catalysts when exposed to small amounts of H_2O,[25−27] and provides key structural data for guiding the growing field of zeolite catalysis in water-rich processes.

RESULTS

Dehydrated HZSM-5 catalysts were prepared in-house via the controlled deammoniation and dehydration of commercial NH_4^+ZSM-5 materials, resulting in one H^+ per framework Al site in the ideal limit. ^{27}Al solid-state NMR is routinely applied to characterize zeolite catalysts, albeit with difficulty in dehydrated catalysts due to large quadrupole coupling constant (C_q) associated with framework Al atoms in distorted symmetries following water removal.[28] At the lower magnetic fields commonly available, typically ca. 14 T and lower, framework signals are broadened beyond recognition due to the large second-order quadrupole coupling broadening, obscuring chemical shift information.[29,30] As such, the vast majority of data in the literature on HZSM-5 catalysts are for hydrated samples. Figure 1 shows ^{27}Al solid-state MAS (magic-angle spinning) NMR data on completely dehydrated HZSM-5 catalysts at relatively high and ultrahigh magnetic field strengths, i.e., 14.1, 19.6, and 35.2 T. As expected, Figure 1 shows that ultrahigh field strength significantly narrows the line widths, allowing general recognition of Al bond orders. However, even at 35.2 T, as shown in Figure 1, it is difficult to unequivocally resolve the features in the 50−60 ppm peak (1a). Aluminum atoms can exist in both framework and extra-framework sites,[31−33] and unequivocally associating Al sites with active Brønsted acid protons is not possible when only detecting Al, even when two-dimensional ^{27}Al multiple-quantum MAS (MQMAS) are used (*vide infra*). The key challenge is to understand the spatial and reactivity relationships between Al and H atoms in both the crystalline and noncrystalline regions of the catalyst in order to identify all potentially active Brønsted sites.

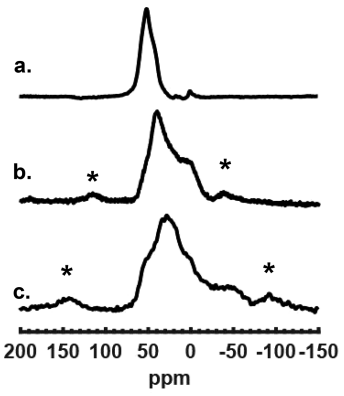

Figure 1. ^{27}Al MAS NMR spectra for dry HZSM-5 catalysts at (a) 35.2, (b) 19.6, and (c) 14 T magnetic field strengths. * denote spinning sidebands.

As general clarification to the reader who is less familiar with NMR of quadrupolar nuclei, it is important to note that the quadrupolar interaction arising from the coupling of the electric quadrupole moment in nuclei with spin quantum number >1/2 to nonspherically symmetric electron distributions around the nucleus can dominate the line shape in randomly oriented powdered solids. This is the case for the ^{27}Al data discussed here, and even in spectra acquired under magic-angle spinning (MAS) conditions, higher-order quadrupolar interactions persist that dominate lineshapes at low magnetic field strengths but become relatively less important at higher fields. For this reason, acquiring data at the highest field strengths possible is important for investigating ^{27}Al siting in catalysts, as reported here for data collected at 35.2 T, as well as comparing those data to data acquired at lower field strengths. For ^{27}Al spins in nonspherical bonding arrangements, e.g., trivalent, pentavalent, or distorted tetrahedral Al, the magnitude of the quadrupolar interaction (denoted as coupling constant C_Q or interaction parameter P_Q) is large and can reach several tens of MHz, obscuring chemical shift information, while those quadrupolar spins involved in tetrahedral or octahedral bonding exhibit reduced or vanishing quadrupolar interactions.

Figure 2 shows the ^{27}Al{^{1}H} Heteronuclear Multiple-Quantum Correlation (HMQC) NMR spectra for the same dehydrated HZSM-5 catalyst shown in Figure 1 acquired using the pulse sequence with dipolar recoupling or D-HMQC sequence.[22−24] Such a sequence has been recently used by Wang et al. to characterize amorphous silica−alumina.[30] Figure 2a shows results obtained at 35.2 T (1500 MHz ^{1}H Larmor frequency), revealing that two distinct tetrahedral Al sites exist with apparent chemical shifts of 51 and 54 ppm, denoted Al(IV)-1 and Al(IV)-2, respectively. The HMQC data show for the first time that Al(IV)-1 and Al(IV)-2 are dipolar-coupled and spatially proximate to two chemically distinct protons at 4.2 and 2.8 ppm, respectively. Al(IV)-1 corresponds to an Al at the well-known BAS, based on extensive literature reporting known ^{27}Al and ^{1}H chemical shift values.[34,35] More important than their different apparent chemical shifts, examination of the line widths of the extracted Al slices shown in the inset of Figure 2a clearly shows that the two tetrahedral Al sites are distinctly different. A comparison of parts c and a of Figure 2 shows that an order of magnitude increase in resolution for the ^{27}Al MAS dimension occurs when acquiring the HMQC data at 35.2 T relative to 14.1 T. More importantly, the presence of the 51/4.2 ppm and 54/2.8 ppm ^{27}Al/^{1}H couplings and their differing field-dependent slices clearly demonstrate that two tetrahedral Al sites exist which are coupled to two protons, thereby excluding a single-site Brønsted model for HZSM-5. For clarity and convenience to the reader, an expanded view of the 35.2 T contour plot in Figure 2a is provided in Figure S1. Most importantly, the 54/2.8 ppm ^{27}Al/^{1}H correlation result for the Al(IV)-2 site has

https://dx.doi.org/10.1021/jacs.0c00590
J. Am. Chem. Soc. 2020, 142, 7514−7523

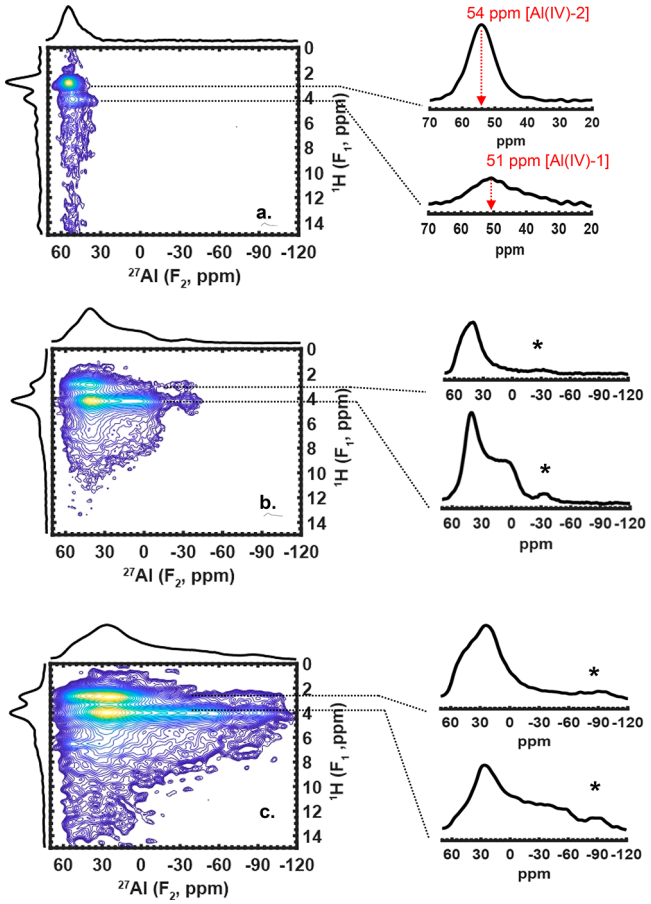

Figure 2. ^{27}Al{^{1}H} D-HMQC MAS NMR spectra for dehydrated HZSM-5 catalysts at (a) 35.2 T, (b) 19.6 T, and (c) 14.1 T. Slices are extracted from the ^{1}H dimension at 2.8 and 4.2 ppm, respectively, and are shown to the right of each contour plot. Note that the scale on the 35.2 T insets in part a covers a much smaller chemical shift range than in parts b or c. The data in part a exclusively reveal the important spatial proximity based on dipolar couplings between the ^{27}Al spins and ^{1}H spins with chemical shifts at 54 and 2.8 ppm, respectively. An expanded view of the contour plot in part a is provided in Figure S1 for convenience to the reader.

implications for understanding catalysis in HZSM-5, as will be discussed in detail below.

Multiple-quantum magic-angle spinning (MQMAS) NMR can identify chemically unique Al atoms in materials.[36] Figure 3 shows variable-field strength ^{27}Al MQMAS spectra for the same dehydrated catalysts as shown in Figures 1 and 2, obtained at 35.2 and 19.6 T. Previously, Kentgens and co-workers have reported ^{27}Al MQMAS data on similar HZSM-5 catalysts at 14 T,[29] and our similar results at that field strength are not presented here for brevity. Figure 3 reveals two Al sites in the tetrahedral region of the spectrum, whose isotropic chemical shifts δ_1 and δ_2, obtained after the application of known methods for shearing and fitting of the second-order quadrupolar induced shifts δ_{qis}, are 55 and 59 ppm for the Al(IV)-1 and Al(IV)-2 sites, respectively.[37,38]

Due to the distribution of both the isotropic chemical shift values and δ_{qis} values, the absolute values of the isotropic chemical shifts δ_1 and δ_2 are less critical than the fact that both shifts are in the known tetrahedral region. However, unlike the ultrahigh field HMQC data in Figure 2, the data in Figure 3 cannot reveal if an Al atom in the catalyst generates a hydroxyl

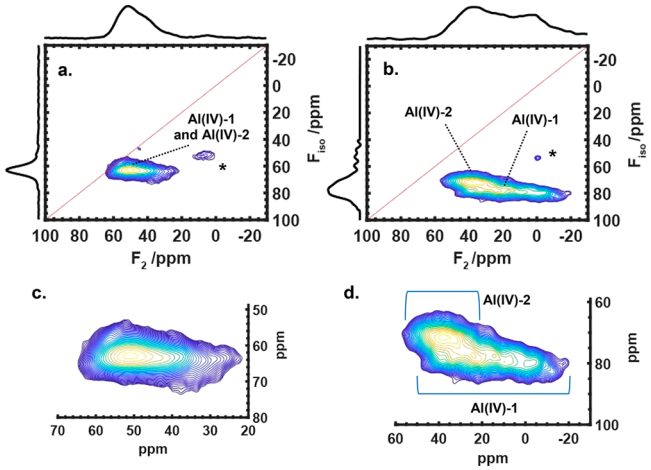

Figure 3. ^{27}Al triple-quantum MAS NMR results for dehydrated HZSM-5 catalysts at (a) 35.2 T and (b) 19.6 T, both acquired at 18 kHz MAS. The asterisks in parts a and b denote a folded first-order sideband, with some residual background contributing to the sideband intensity in part b. Expansions of the catalyst signal regions in parts a and b are shown in parts c and d, respectively. At 19.6 T, Al(IV)-1 and Al(IV)-2 are well resolved while at 35.2 T, both aluminum sites converge into one peak due to negligible δ_{qis}, further demonstrated in Figure S5. Notably, the Al(IV)-2 line width exceeds that of Al(IV)-1 in the isotropic F1 dimension, as also observed in the HMQC data. Spectra are plotted following the shearing transformation in F1.

proton site. Table 1 summarizes key parameters obtained from fitting the multiple-magnetic field data in Figures 1−3,

Table 1. Quadrupolar and Chemical Shift Parameters for the Al(IV)-1 and Al(IV)-2 Sites Determined via Fitting of the Single-Pulse, HMQC, and MQMAS Data in Figures 1−3 and in the SI[a]

	Al(IV)-1	Al(IV)-2
Chemical shift distribution (ppm)	≤7	∼8
P_q (MHz)	17	11
δ_{iso} (ppm)	55	59
η_Q	0.1	0.6

[a]P_q = quadrupolar interaction product; δ_{iso}= isotropic chemical shift value; η_Q = quadrupole asymmetry parameter.

including both HMQC and MQMAS data, with additional details given in Figures S2−S5 and Table S1. Key outcomes are that the Al(IV)-2 species, which hosts the hydroxyl group giving rise to the 2.8 ppm ^{1}H signal, has an ^{27}Al isotropic shift that is clearly in the tetrahedral chemical shift region and also exhibits a larger quadrupole asymmetry parameter but a smaller quadrupole coupling constant C_Q than the BAS Al(IV)-1 site. As a control, we note that the η = 0.1 for the Al(IV)-1 in the BAS agrees with previous reports[29,46] and also with the calculated values from theory which are described along with computational support for other experimental results below.

DISCUSSION

Many publications report that the most active forms of zeolite catalysts in general, and HZSM-5 in particular, contain more than just isolated crystalline BASs.[2,11,14,15,39,40] However, the identification of structural moeties other than BASs that contribute to enhanced catalyst function is still a lively topic of

https://dx.doi.org/10.1021/jacs.0c00590
J. Am. Chem. Soc. 2020, 142, 7514−7523

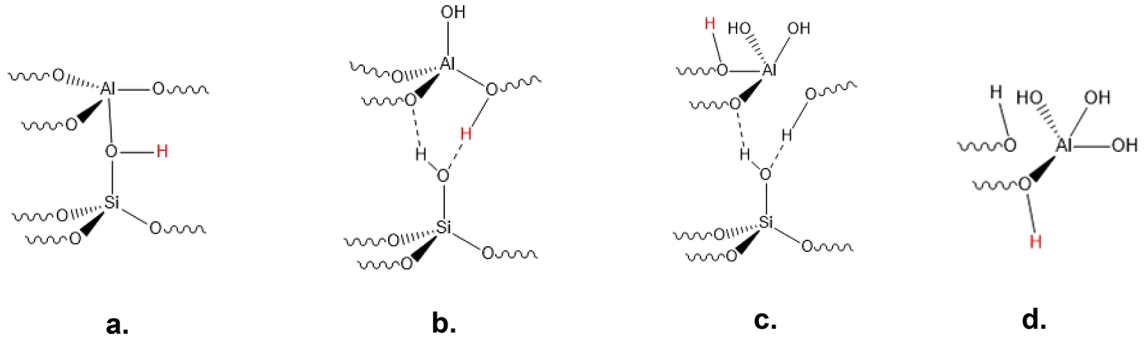

Figure 4. Schematics depicting (a) the well-known BAS in the zeolite lattice, and intermediate structures formed via attack of (b) one, (c) two, and (d) three water molecules at the BAS. The Al atoms in structures b–d are representative of the Al(IV)-2 species.

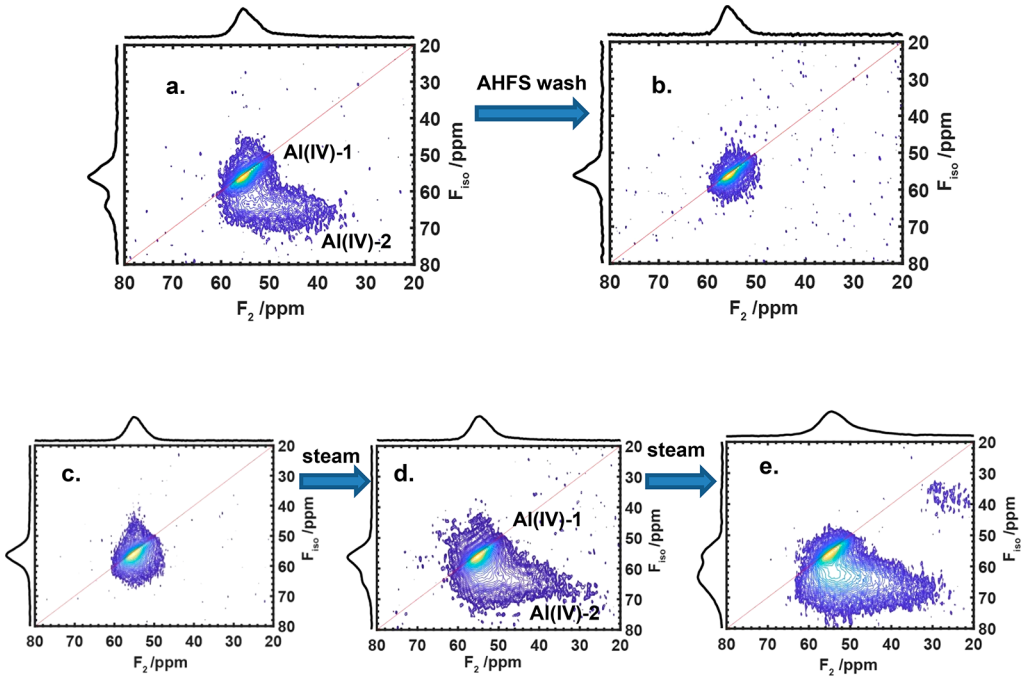

Figure 5. ^{27}Al triple-quantum MAS NMR results at 14 T for hydrated HZSM-5 catalysts as a function of postsynthetic treatments: (a) HZSM-5 with Si/Al = 15; (b) same as in part a, following AHFS washing; (c) HZSM-5 with Si/Al = 11.5; (d) same as in part c, following a mild steam treatment; (e) same as is in part c, following a severe steam treatment. Details of AHFS washing and steaming treatments are described in the SI. Figure S5 shows data for the sample in part a obtained at four different magnetic field strengths under ambient hydration, demonstrating that the Al(IV)-2 signal cannot be an artifact nor can it arise from trivalent Al species.

debate, with multiple papers appearing in current literature focusing on "synergistic" effects arising from nearest neighbor or proximate framework BASs,[18,39,41] Brønsted-Lewis synergies,[40,41] and Brønsted-Brønsted synergies.[19,44,45] The two latter categories include interactions between framework BASs and nonframework species. The general consensus is that nonframework species are of the general structure $Al_x(OH)_y$, free from the bonding constraints of the lattice, and can migrate or block channels. The Al atom in EFAl (extra-framework aluminum) species is a Lewis acid, and many reports propose that the EFAl species proximate to a BAS increases the reactivity of the latter via a Brønsted-Lewis synergy.[2,42,43] Hydrothermal treatments of zeolites increase the population of EFAl species through high-temperature water attack at Al tetrahedra in the lattice, which coincides with increased catalyst activity in high-temperature (ca. 500 °C) probe reactions like cumene cracking as demonstrated many times for Y-type zeolites.[2,43] Other groups, particularly in the context of lower-temperature reactions, have shown that Brønsted-Brønsted synergies between BASs and nonframework aluminols increase catalyst activity,[19] with some computational reports even calling into question the existence of Brønsted-Lewis synergies altogether in some zeotypes.[44,45] NMR spectroscopy has played a key role in trying to understand structure and reactivity relationships in the context of catalyst synthesis and postsynthetic treatments, with the observation of Al (IV) signals in the known tetrahedral 50–65 ppm region vs Al(VI) signals near 0 ppm as the most commonly employed marker of BAS framework Al and EFAl in HZSM-5 catalysts, respectively.[38,46,47] The limitations of the detection of signals from quadrupolar Al atoms in nonspherical bonding environments are well-known, which is why the majority of data in literature is centered on hydrated HZSM-5 catalysts. Similarly, signals at 4.0–4.5 and 2.5–2.9 ppm in ^{1}H solid-state NMR spectra of dehydrated HZSM-5 have been used as indicators of hydroxyl groups on BAS and EFAl species, respectively.[35,46] Thus, the presence of a 2.8 ppm signal in the proton spectrum or the proton dimension of a 2D heteronuclear correlation

https://dx.doi.org/10.1021/jacs.0c00590
J. Am. Chem. Soc. 2020, 142, 7514–7523

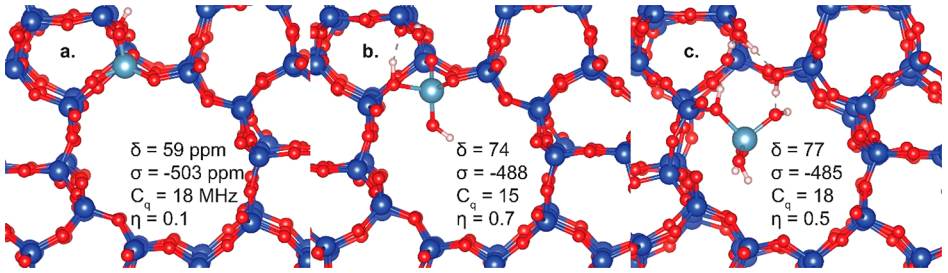

Figure 6. Calculated DFT structures for (a) an isolated BAS containing only Al(IV)-1, and the partially bonded Al(IV)-2 structure resulting from addition of (b) one water and (c) three waters to structure in part a. Absolute chemical shielding values σ are in ppm units, quadrupole coupling constant C_q in MHz, and the asymmetry parameter η is unitless.

spectrum would indicate hydroxyl groups from EFAl species, based on historical literature assignments.

The dipolar HMQC data in Figure 2 shows that a tetrahedral Al atom with a signal at 51 ppm at 35.2 T is coupled to a ^{1}H whose signal appears at 4.2 ppm. This correlation arises from the framework BAS involving Al(IV)-1 and its bridging hydroxyl proton, as shown in Figure 4a, and is expected. The known values for the BAS serve as important internal calibration. Conversely, the correlation between the 54 ppm Al(IV)-2 signal and the 2.8 ppm ^{1}H signal is not expected, since that ^{27}Al signal clearly arises from an aluminum atom in a tetrahedral bonding environment, and the literature assigns the 2.8 ppm ^{1}H signal to hydroxyls on EFAl species that are not tetrahedral Al(IV), but rather Al(III), Al(V), or Al(VI).[35,46] Recent literature indicates that the protons giving rise to the 2.8 ppm signal are themselves reactive, and when removed from the catalyst using known methods for zeolite EFAl extraction like ammonium hexafluorosilicate (AHFS) washing, overall reaction rates decrease.[14,15,19,48] AHFS washing, under appropriate conditions, can selectively remove Al that is not associated with a framework BAS while leaving BASs intact, thereby generating a "clean" catalyst.[14,15,19] Previously, it has been shown that the 2.8 ppm signal for HZSM-5 catalysts can be completely removed by mild AHFS washing and then reintroduced when the washed catalyst is subjected to wet flowing air at ca. 500 °C, i.e., steaming.[40] Similarly, the MQMAS ^{27}Al spectra in Figure 5 demonstrate that the Al(IV)-2 signal behaves in an identical fashion, i.e., it is removed by mild AHFS washing (5a,b), and reintroduced by steaming (5c−e). In addition to the spectroscopic correlation of signals for the Al(IV)-2 species in the HMQC as seen via the 54/2.8 ppm cross ^{27}Al/^{1}H peaks, there is also a chemical correlation due to the fact that both signals respond in an identical fashion to postsynthetic AHFS treatments.

It is important to point out that the HMQC correlations between Al(IV)-2 and its ^{1}H signal do not mean that the only protons associated with Al(IV)-2 are weakly acidic, as suggested by the low ^{1}H chemical shift value of 2.8 ppm. The charge-balancing proton created by Al(IV)-2, shown in red in Figure 4, will likely exhibit a broad chemical shift range due to its complex hydrogen bonding environment. Figure S6 shows that the dry initial catalyst, prior to AHFS washing or any steaming, exhibits a broad signal from 12 to 15 ppm in addition to a broad 5−7 ppm signal. As previously shown,[14,19] these signals, along with the 2.8 ppm signal, are removed by AHFS washing. The 2.8 ppm and 12−15 ppm ^{1}H signals are detected together as long as the catalyst is sufficiently dry; trace moisture leads to chemical exchange for the acidic 12−15 ppm signal protons. Since the 12−15 ppm signal is weak, its clear resolution is difficult in the HMQC data of Figure 2. The fact that the hydroxyl groups generating the 2.8 ppm and 12−15 ppm hydroxyl groups are simultaneously proximate is proven by the ^{1}H−^{1}H DQSQ data shown in Figure S7 for the dry HZSM-5 catalyst, in which their specific correlation is observed at the double-quantum frequency shown by the summed chemical shift at (2.8 ppm +12.5 ppm) = 15.3 ppm in the selected slice. Similarly, the entire broad 12−15 ppm signal is correlated with the 2.8 ppm signal, giving a range in the double-quantum axis. In total, these data in concert with the DFT quadrupolar parameters in Figure 6 and chemical shift calculations in Figures S9−S11 (*vide infra*) are consistent with the proposed structures in Figure 4b−d.

The combined spectroscopic and postsynthetic catalyst treatment results indicate that the Al(IV)-2 species, and its ^{1}H-containing hydroxyl groups, are associated with the framework as partially hydrolyzed but still partially bonded Brønsted site of the types shown in Figure 4b−d. The Al(IV)-2 Brønsted protons are denoted by red in Figure 4b−d, and by definition, they must exist if associated with a hydroxyl group on an Al(IV) atom due to charge balance requirements. Previously, Kentgens assigned an Al(IV)-2 species in an HZSM-5 catalyst to framework BAS Al species perturbed by cations like Na^+, or to EFAl.[29] However, that does not agree with our HMQC correlation data in this case since Al(IV)-2 is correlated to Al−OH that is removed by AHFS, and created by steaming, as described above. It is important to recognize that both the Al(IV)-2 ^{27}Al signal and its associated ^{1}H signal are observed in the absence of a 0 ppm Al(VI) or a 30−40 ppm Al(V) signal in dehydrated catalysts. Figure S8 shows additional comparative data for Si/Al = 11.5, including the full chemical shift range as a function of catalyst history that indicates that Al(III) or Al(V) is never present in detectable amounts unless the catalyst is steamed.

Further evidence supporting the assignment of an active Brønsted site at partially bonded Al(IV)-2 species comes from DFT calculations shown in Figure 6 with additional calculated structures in Figures S9−S11.[51,52] The absolute chemical shift tensor of Al in aluminum acetylacetonate $Al(acac)_3$ was calculated for a reference, yielding a value of −562 ppm. Using this as the reference, the chemical shift of Al in Figure 6 can be converted to 59, 74, and 77 ppm for the intrinsic site, the one with one water incorporated and the one with three water in the structure, respectively. The chemical shift of Al is very sensitive to the local distortion as shown in Figure S9; the chemical shift of the Al at the early stage of hydrolysis (one water incorporated) could range from 65 to 74 ppm or an uncertainty in the chemical shift calculation on the order of 10 ppm. The chemical shift trends caused by partial hydrolysis

https://dx.doi.org/10.1021/jacs.0c00590
J. Am. Chem. Soc. 2020, 142, 7514−7523

Table 2. Comparison of Conversion and Reaction Rate Data As a Function of Al(IV)-1 and Al(IV)-2 Species, and Their Associated OH Group Concentrations[a]

Catalyst	Al(IV)-1 (mmol/g) (a)	4.2 ppm BAS OH signal (mmol/g) (b)	Al(IV)-2 (mmol/g) (b)	2.8 ppm of OH signal (mmol/g) (b)	total Bronsted acidity (mmol/g) (c)	normalized *n*-hexane conversion per μmole Bronsted site (d)	normalized H/D exchange rate constant for benzene reaction (s^{-1}) (e)
Dry Si/Al = 15	~0.67	0.56 ± 0.018	~0.23	0.09 ± 0.01	0.73	3%	23
Dry Si/Al = 15 after AHFS wash	~0.60	0.54 ± 0.020	~0.06	0.030 ± 0.003	0.70	0.6%	1
Dry Si/Al = 11.5		0.61 ± 0.02		0.05 ± 0.01	1.08	1.3%	

[a](a) From elemental analysis and quantitative ^{27}Al NMR (b) from quantitative ^{1}H spin-counting NMR data; (c) from IPA TPD measurements; (d) from pulsed-microreactor data at 480°C with GC/MS detection; (e) from room-temperature in-situ NMR of benzene-d_6/HZSM-5 exchange reaction.

agree with the experimental results in Table 1 and Figures 2 and 3, though the calculated changes (6−15 ppm) are larger than the experimental value of 4 ppm.

Figure 6 shows calculated structures for two of the four species shown above in Figure 4, with chemical shift and shielding information, quadrupole coupling constant C_Q, and asymmetry parameter η_Q reported in the figure. While there can be deviations in absolute values of any of these parameters based on small changes in bond angles surrounding any Al center, the trends are in close agreement with the experimental data reported above. A comparison of the BAS Al(IV)-1 in 6a with that of the Al species in 6b, for example, shows that the latter Al species in a partially bonded framework position has reduced chemical shielding by ca. 12 ppm (i.e., larger chemical shift), a smaller C_Q, and a larger η_Q. Recall, the Al(IV)-2 experimental data summarized in Table 1 shows a larger chemical shift by 3−4 ppm, a smaller C_q by +6 MHz, and η_Q = 0.6 versus 0.1 for the BAS Al(IV)-1. Figure 6b shows the structure resulting from one water of addition at the BAS, and similar trends are observed after addition of three water molecules. The value of C_Q is very sensitive to local disorder. Conversely, as shown in Figure S10, ^{27}Al chemical shift and quadrupolar parameters for trivalent Al(III) species of the type commonly associated with extra-framework Al are completely inconsistent with the experimental data for the Al(IV)-2 species discussed above. Other Al(IV) configurations following addition of one water molecule are shown in Figure S9. In addition, Figure S11 shows the calculated results for ^{1}H chemical shifts, exhibiting the well-known isolated BAS signal near the experimental 4.2 ppm as well as other shifts significantly downfield in the 11−16 ppm region which also agree with recently reported experimental shifts in the 12−15 ppm region for HZSM-5.[14,19,40]

Additional key evidence for the role of partially bonded framework structures as the source of Al(IV)-2 comes from the examination of ^{29}Si NMR of HZSM-5. Figure S12 shows that a small amount of Si with one adjacent Al(IV) is removed following AHFS treatment. However, previous publications show that BAS hydroxyl groups are not perturbed, which must occur if a BAS Al is extracted.[14,15] Those same publications show that signals traditionally assigned to EFAl OH's, i.e., the 2.8 ppm peak in the ^{1}H MAS NMR spectra, are attenuated or completely eliminated as recently reported.[14,15,19,40] Also, there is no apparent correlation between the presence of a 0 ppm Al(VI) peak in Al MAS NMR data and the 2.8 ppm peak in ^{1}H NMR data; strong 2.8 ppm peaks are routinely observed in the absence of a 0 ppm Al(VI) signal. All of these inconsistencies are explained by a contribution from the structures in Figure 4 that are experimentally confirmed by the 35.2 T HMQC data in Figure 2 and the supporting analyses described herein. Such structures would be more susceptible to attack by AHFS than framework BASs, similar to what has been observed for EFAl species. These same structures are predicted by the computational analysis of the partial hydrolysis products in zeolites subjected to dealumination steps, as reported recently, and would also be present from incomplete framework condensation during synthesis, particularly for the high-Al content zeolites discussed here.[49,50]

Al(IV)-2 Impact on Catalysis. Table 2 summarizes the relationship between catalyst reactivity and the relative amounts of traditional BAS arising from Al(IV)-1 and its associated bridging hydroxyl group versus that of Al(IV)-2 and its hydroxyl groups. This table should be viewed along with ^{1}H and ^{27}Al spectra in Figures S6 and S13 along with Figure 2 that demonstrates the H−Al correlations. Pulsed microreactor conversions of *n*-hexane at 480 °C were used to measure the activity of catalysts under very low conversion conditions, less than 12%, to emphasize primary reaction steps and limit secondary reactions, the details for which have been previously described and are also found in the SI.[19] No catalyst deactivation was observed. The product distribution, shown in Figure S14, is comparable with previously reported selectivity.[53] The activities of the catalysts do not depend in a straightforward way on the amount of total Brønsted acidity as measured by traditional IPA TPD. As shown in Table 2, the Si/Al = 11.5 catalyst has more BAS and total acidity than the 15 catalyst but exhibits less than half of the latter's conversion. The washing of the Si/Al = 15 catalyst with AHFS under mild conditions does not significantly impact the total amount of Al(IV)-1 or its BAS proton concentration as shown in the third column of Table 2, but it does significantly reduce the Al(IV)-2 and its associated hydroxyl group, as shown in the fourth and fifth column. Catalysts prepared in this way have the lowest conversion for *n*-hexane and also the lowest H/D exchange rate constant in room temperature reactions with benzene-d_6 as shown in the last two columns. Again, the data shown in Figures 3, 5, S6, and S13 clearly indicate that reactivity depends on variations in the new Al(IV)-2 species discussed here, and not detectable variations in Al(III), Al(V), and Al(VI) species. While such variations may exist, the magnitude of the original amount of Al(IV)-2 and its changes with catalyst selection or post-treatment are much larger than any of the aforementioned species and also larger than any changes in Al(IV)-1 and its BAS proton concentration and therefore cannot be ignored.

https://dx.doi.org/10.1021/jacs.0c00590
J. Am. Chem. Soc. 2020, 142, 7514−7523

Summary of Evidence for Al(IV)-2 Identification and Structure Assignment. Al(IV)-2 cannot be assigned to traditional EFAl species, i.e., Al(III), Al(V), or Al(VI) for the following reasons. First, the second type of Al(IV) described here is an Al atom that is tetrahedrally bonded to four oxygen atoms, based on known chemical shift and C_Q data, thus possessing a negative formal charge. Al(IV)-2 cannot be a Lewis acid, since it has a negative formal charge. Dimers or trimers of a nonframework $Al(OH)_4^-$ would also be negatively charged and would thus be unable to function as Lewis acids. Second, due to the requisite Al(IV) charge, a proton associated with it is required as indicated in Figure 4. Figures 2, S6, and S13 show that the Al(IV)-2 species and its hydroxyl group are the key varying structural moieties in these catalysts based on preparation and postsynthetic treatments. Figures S9 and S10 demonstrate that the quadrupolar parameters for Al(IV)-2 are significantly different than those for Al(III) species. Finally, the new Al(IV)-2 reported here is bonded to a Si atom, as shown by the data in Figure S12, which shows it is associated with the framework and cannot be assigned to extraframework species. Most importantly, as shown in Figure 3a,b, Al(IV)-2 is detected prior to any extraframework Al(V) or Al(VI) species in the dry catalysts, the latter of which gives rise to the known ca. 30 and 0 ppm signals that are typically used as evidence for dealumination. No signals are observed at 0 or 30 ppm in Figure 3 for the dry catalysts. The structure and chemical relevance of tetrahedrally coordinated Al(IV)-2 cannot be attributed to EFAl and exists in the absence of detectable ^{27}Al signals arising from EFAl, as shown for the unsteamed and untreated NH4ZSM-5 sample in Figure S15.

To our knowledge, partially bonded Al(IV) has been previously proposed based on theory[49] but without experimental evidence showing that it can be an active species in zeolites. The experimental data presented here shows direct evidence for their existence and catalytic relevance. Previous works by Prins and Bokhoven discussing partially dislodged Al referred to octahedral aluminum and involved either β or Y-type zeolites.[55−57] From that work, it appears that only Al(VI) can be reinserted to the framework by NH_3 treatment and not Al(IV). In recent work, framework-associated Al(VI) Lewis sites were reported in mordenite or as dislodged Al(IV) that was hydrated.[54,56] The previous MQMAS work by Kentgens describing a second Al(IV) site in MFI likely detected the same species reported as Al(IV)-2 in our MQMAS data, albeit without the structural insight afforded by the HMQC and other solid-state NMR data reported here for dry catalysts.[29] The structures discussed in previous contributions are not the same as the Al(IV)-2 species proposed here, as Figure S12 indicates that Al(IV)-2 is chemically bonded to Si atoms. For the MFI samples used in our work, it is reasonable that partially bonded Al(IV)-2 forms before extra-framework Al species form. As can be seen in the attached full chemical shift range of ^{27}Al MQMAS, Figure S8, Al(V) can of course be formed and detected after severe hydrothermal treatment, but Al(IV)-2 is logically formed earlier than Al(V).

Summary of Al Sites in Hydrated vs Dehydrated Catalysts. The data show that Al(IV)-2 has the higher chemical shift and smaller P_q relative to those of Al(IV)-1 in the dehydrated catalysts but a larger P_q and apparent lower chemical shift in the hydrated catalysts. Upon hydration, it is known that the Al(IV)-1 site is surrounded by clusters of water molecules that delocalize the H^+ charge through rapid chemical exchange, and since Al is bonded to four Si atoms via oxygen bridges, near-tetrahedral geometry results in a negligible electric field gradient and detectable Al NMR spectra under normal acquisition conditions. Conversely, when water is removed from Al(IV)-1, the localized charge and concomitant lattice strain resulting from bonding to fixed framework Si−O moieties is significant, leading to large P_q values of the magnitude shown in Table 1. In all cases, Al(IV)-1 is bonded via oxygen bridges to four framework Si atoms, and thus the 55-ppm isotropic chemical shift does not change significantly as a function of hydration. Al(IV)-2, by virtue of the fact that it is bonded to both framework SiO moieties and hydroxyl groups as in Figure 6b,c, maintains a significant electric-field gradient upon hydration due to interactions between the hydroxyl groups and water molecules. An apparent lower chemical shift for Al(IV)-2 relative to Al(IV)-1 in the hydrated case shown in Figure 5 results from the large δ_{qis} for the former. D-HMQC experiments of the type shown in Figure 2 for the dehydrated cases are not reliable for fully hydrated catalyst samples due rapid proton chemical exchange which is well-known to occur; such experiments will emphasize only the most rigid Al−H pairs.

Relevance of Al(IV)-2 to Location, Topology, and Proximity Contributions to Catalyst Reactivity. Contributions from Iglesia, Bell, and Lercher, among others, have recently shown that catalyst activity can depend on several factors, including active site location,[12,15] channel structures and their chemical composition,[58−62] and proximity to EFAl species.[63] Very recent work by Lercher's group suggests that the creation of BASs with proximate EFAl species contributes more significantly to increased catalyst activity.[64] In each of these works, where proximate EFAl effects contribute, strong and intense signals in the Al NMR at either 0 or ca. 30 ppm are observed following specific steaming protocols. It is important to note that in our work, only Al(IV)-1 and Al(IV)-2 signals are observed in the 50−60 ppm region of the spectrum in catalysts that have not been steamed; EFAl signals are not observed as can be seen in Figure 3 on dry HZSM-5 prior to any treatments, even at the highest 35.2 T field strength shown by 3a. Also, there is a lack of EFAl signals, but a significant Al(IV)-2 signal is shown in Figure S15, which was obtained on an unexchanged NH_4^+ZSM5 sample. Unsteamed and untreated catalysts that have both Al(IV)-1 and Al(IV)-2 sites, with their associated hydroxyl groups, are more active in the cracking and H/D exchange reactions discussed above than the catalysts that have only the traditional isolated BAS created by Al(IV)-1, as shown by the data in Table 2. These results in no way preclude any of the enhancements afforded by the EFAl species once they are formed, as discussed in the references cited immediately above. Rather, they afford additional atomistic detail of framework contributions to reactivity that are more complex than can be attributed to a single type of framework acid site. These must be considered further when trying to fully predict the impact of synergistic EFAl effects since Al(IV)-2 sites can ultimately generate EFAl species after steaming.

CONCLUSIONS

In summary, the ultrahigh magnetic field data and supporting computational data reveal that zeolites can have at least two types of chemically distinct tetrahedral aluminum atoms associated with the zeolite framework, thereby creating the possibility for two chemically distinct Brønsted sites. The room-temperature H/D exchange experiments and the high-

https://dx.doi.org/10.1021/jacs.0c00590
J. Am. Chem. Soc. 2020, 142, 7514−7523

temperature *n*-hexane cracking experiments indicate that Al(IV)-2 and its accompanying hydroxyl groups increase catalyst activity relative to catalysts that only contain Al(IV)-1 and its associated BAS. The observed results cannot be easily attributed to Al atoms in nonframework species, as the latter were in most cases not detected or detected in trace amounts well below those of the partially coordinated Al(IV)-2 sites. The data suggest that the collective understanding and practical implementation of zeolite-based catalysis can include synthetic and postsynthetic modification to target these partially coordinated framework Al(IV) sites, potentially leading to increased catalytic activity and longevity through the strategic use of water, as will be explored in future work.

■ ASSOCIATED CONTENT

Supporting Information

The Supporting Information is available free of charge at https://pubs.acs.org/doi/10.1021/jacs.0c00590.

Experimental methods and their supporting references; details of fittings, simulations, and calculations; results from DFT calculations; ^{1}H and ^{29}Si solid-state NMR spectra; and static ^{27}Al 1D and MQMAS spectra (PDF)

■ AUTHOR INFORMATION

Corresponding Authors

Jeffery L. White − *School of Chemical Engineering, Oklahoma State University, Stillwater, Oklahoma 74078, United States;* orcid.org/0000-0003-4065-321X; Email: jeff.white@okstate.edu

Kuizhi Chen − *National High Magnetic Field Laboratory, Tallahassee, Florida 32310, United States;* Email: kuizhi.chen@magnet.fsu.edu

Authors

Sarah Horstmeier − *Department of Chemistry, Oklahoma State University, Stillwater, Oklahoma 74078, United States*

Vy. T. Nguyen − *School of Chemical, Materials, and Biological Engineering, University of Oklahoma, Norman, Oklahoma 73019, United States*

Bin Wang − *School of Chemical, Materials, and Biological Engineering, University of Oklahoma, Norman, Oklahoma 73019, United States;* orcid.org/0000-0001-8246-1422

Steven P. Crossley − *School of Chemical, Materials, and Biological Engineering, University of Oklahoma, Norman, Oklahoma 73019, United States*

Tram Pham − *School of Chemical, Materials, and Biological Engineering, University of Oklahoma, Norman, Oklahoma 73019, United States*

Zhehong Gan − *National High Magnetic Field Laboratory, Tallahassee, Florida 32310, United States*

Ivan Hung − *National High Magnetic Field Laboratory, Tallahassee, Florida 32310, United States*

Complete contact information is available at: https://pubs.acs.org/10.1021/jacs.0c00590

Notes

The authors declare no competing financial interest.

■ ACKNOWLEDGMENTS

This material is based upon work supported by the National Science Foundation under Grant Nos. CHE-1764116 and CHE-1764130, and are gratefully acknowledged. Partial instrumentation support for the solid-state NMR system at Oklahoma State University was provided in part through the Oklahoma State University Core Facilities program. Development of the SCH magnet and NMR instrumentation was supported by NSF (DMR-1039938 and DMR-0603042). The operations of the SCH magnet and the NMR Spectroscopy operations are overseen respectively by the DC User Facility and the NMR and MRI User Facility at the NHMFL that is supported by NSF DMR-1157490 and the State of Florida. The user activities of the SCH are further supported by NIH P41 GM122698.

■ REFERENCES

(1) Trickett, C. A.; Osborn Popp, T. M.; Su, J.; Yan, C.; Weisberg, J.; Huq, A.; Urban, P.; Jiang, J.; Kalmutzki, M. J.; Liu, Q.; Baek, J.; Head-Gordon, M. P.; Somorjai, G. A.; Reimer, J. A.; Yaghi, O. M. Identification of the strong Brønsted acid site in a metal-organic framework solid acid catalyst. *Nat. Chem.* **2019**, *11* (2), 170−176.

(2) Haag, W. O.; Lago, R. M.; Weisz, P. B. The active site of acidic aluminosilicate catalysts. *Nature* **1984**, *309*, 589.

(3) Xu, B.; Sievers, C.; Hong, S. B.; Prins, R.; van Bokhoven, J. A. Catalytic activity of Brønsted acid sites in zeolites: Intrinsic activity, rate-limiting step, and influence of the local structure of the acid sites. *J. Catal.* **2006**, *244* (2), 163−168.

(4) Kissin, Y. V. Chemical Mechanisms of Catalytic Cracking Over Solid Acidic Catalyst: Alkanes and Alkenes. *Catal. Rev.: Sci. Eng.* **2001**, *43* (1−2), 85−146.

(5) Corma, A. Inorganic Solid Acids and Their Use in Acid-Catalyzed Hydrocarbon Reactions. *Chem. Rev.* **1995**, *95* (3), 559−614.

(6) Ennaert, T.; Van Aelst, J.; Dijkmans, J.; De Clercq, R.; Schutyser, W.; Dusselier, M.; Verboekend, D.; Sels, B. F. Potential and challenges of zeolite chemistry in the catalytic conversion of biomass. *Chem. Soc. Rev.* **2016**, *45* (3), 584−611.

(7) Zapata, P. A.; Faria, J.; Ruiz, M. P.; Jentoft, R. E.; Resasco, D. E. Hydrophobic Zeolites for Biofuel Upgrading Reactions at the Liquid-Liquid Interface in Water/Oil Emulsions. *J. Am. Chem. Soc.* **2012**, *134* (20), 8570−8578.

(8) Corma, A.; Orchillés, A. V. Current Views on the Mechanism of Catalytic Cracking. *Microporous Mesoporous Mater.* **2000**, *35*−*36*, 21−30.

(9) Tian, P.; Wei, Y.; Ye, M.; Liu, Z. Methanol to Olefins (MTO): From Fundamentals to Commercialization. *ACS Catal.* **2015**, *5* (3), 1922−1938.

(10) Ilias, S.; Bhan, A. Mechanism of the Catalytic Conversion of Methanol to Hydrocarbons. *ACS Catal.* **2013**, *3* (1), 18−31.

(11) Knott, B. C.; Nimlos, C. T.; Robichaud, D. J.; Nimlos, M. R.; Kim, S.; Gounder, R. Consideration of the Aluminum Distribution in Zeolites in Theoretical and Experimental Catalysis Research. *ACS Catal.* **2018**, *8* (2), 770−784.

(12) Jones, A. J.; Carr, R. T.; Zones, S. I.; Iglesia, E. Acid strength and solvation in catalysis by MFI zeolites and effects of the identity, concentration and location of framework heteroatoms. *J. Catal.* **2014**, *312* (0), 58−68.

(13) Pashkova, V.; Sklenak, S.; Klein, P.; Urbanova, M.; Dědeček, J. Location of Framework Al Atoms in the Channels of ZSM-5: Effect of the (Hydrothermal) Synthesis. *Chem. - Eur. J.* **2016**, *22* (12), 3937−3941.

(14) Chen, K.; Abdolrhamani, M.; Sheets, E.; Freeman, J.; Ward, G.; White, J. L. Direct Detection of Multiple Acidic Proton Sites in Zeolite HZSM-5. *J. Am. Chem. Soc.* **2017**, *139* (51), 18698−18704.

(15) Schallmoser, S.; Ikuno, T.; Wagenhofer, M. F.; Kolvenbach, R.; Haller, G. L.; Sanchez-Sanchez, M.; Lercher, J. A. Impact of the local environment of Brønsted acid sites in ZSM-5 on the catalytic activity in n-pentane cracking. *J. Catal.* **2014**, *316*, 93−102.

(16) Li, C.; Vidal-Moya, A.; Miguel, P. J.; Dedecek, J.; Boronat, M.; Corma, A. Selective Introduction of Acid Sites in Different Confined

Positions in ZSM-5 and Its Catalytic Implications. *ACS Catal.* **2018**, *8* (8), 7688−7697.
(17) Perea, D. E.; Arslan, I.; Liu, J.; Ristanovic, Z.; Kovarik, L.; Arey, B. W.; Lercher, J. A.; Bare, S. R.; Weckhuysen, B. M. Determining the location and nearest neighbours of aluminium in zeolites with atom probe tomography. *Nat. Commun.* **2015**, *6*, 8589.
(18) Song, C.; Chu, Y.; Wang, M.; Shi, H.; Zhao, L.; Guo, X.; Yang, W.; Shen, J.; Xue, N.; Peng, L.; Ding, W. Cooperativity of adjacent Brønsted acid sites in MFI zeolite channel leads to enhanced polarization and cracking of alkanes. *J. Catal.* **2017**, *349*, 163−174.
(19) Chen, K.; Abdolrahmani, M.; Horstmeier, S.; Pham, T. N.; Nguyen, V. T.; Zeets, M.; Wang, B.; Crossley, S.; White, J. L. Brønsted-Brønsted Synergies between Framework and Noncrystalline Protons in Zeolite H-ZSM-5. *ACS Catal.* **2019**, *9* (7), 6124−6136.
(20) Gounder, R.; Jones, A. J.; Carr, R. T.; Iglesia, E. Solvation and acid strength effects on catalysis by faujasite zeolites. *J. Catal.* **2012**, *286*, 214−223.
(21) Gan, Z.; Hung, I.; Wang, X.; Paulino, J.; Wu, G.; Litvak, I. M.; Gor'kov, P. L.; Brey, W. W.; Lendi, P.; Schiano, J. L.; Bird, M. D.; Dixon, I. R.; Toth, J.; Boebinger, G. S.; Cross, T. A. NMR spectroscopy up to 35.2T using a series-connected hybrid magnet. *J. Magn. Reson.* **2017**, *284*, 125−136.
(22) Lafon, O.; Wang, Q.; Hu, B.; Vasconcelos, F.; Trébosc, J.; Cristol, S.; Deng, F.; Amoureux, J.-P. Indirect Detection via Spin-1/2 Nuclei in Solid State NMR Spectroscopy: Application to the Observation of Proximities between Protons and Quadrupolar Nuclei. *J. Phys. Chem. A* **2009**, *113* (46), 12864−12878.
(23) Trebosc, J.; Hu, B.; Amoureux, J. P.; Gan, Z. Through-space R3-HETCOR experiments between spin-1/2 and half-integer quadrupolar nuclei in solid-state NMR. *J. Magn. Reson.* **2007**, *186*, 220−227.
(24) Hu, B.; Trebosc, J.; Amoureux, J. P. Comparison of several heteronuclear dipolar recoupling NMR methods to be used in MAS HMQC/HSQC. *J. Magn. Reson.* **2008**, *192*, 112−122.
(25) Xue, N.; Vjunov, A.; Schallmoser, S.; Fulton, J. L.; Sanchez-Sanchez, M.; Hu, J. Z.; Mei, D.; Lercher, J. A. Hydrolysis of zeolite framework aluminum and its impact on acid catalyzed alkane reactions. *J. Catal.* **2018**, *365*, 359−366.
(26) Chen, K.; Damron, J.; Pearson, C.; Zhang, L.; Resasco, D.; White, J. L. Zeolite Catalysis: Water Can Dramatically Increase or Suppress Alkane C-H Bond Activation. *ACS Catal.* **2014**, *4*, 3039−3045.
(27) Motokura, K.; Matsunaga, S.; Noda, H.; Miyaji, A.; Baba, T. Water-Accelerated Allylsilylation of Alkenes Using a Proton-Exchanged Montmorillonite Catalyst. *ACS Catal.* **2012**, *2* (9), 1942−1946.
(28) Grey, C. P.; Vega, A. J. Determination of the Quadrupole Coupling Constant of the Invisible Aluminum Spins in Zeolite HY with 1H/27Al TRAPDOR NMR. *J. Am. Chem. Soc.* **1995**, *117* (31), 8232−8242.
(29) Kentgens, A. P. M.; Iuga, D.; Kalwei, M.; Koller, H. Direct Observation of Brønsted Acidic Sites in Dehydrated Zeolite H-ZSM5 Using DFS-Enhanced 27Al MQMAS NMR Spectroscopy. *J. Am. Chem. Soc.* **2001**, *123* (12), 2925−2926.
(30) Wang, Z.; Jiang, Y.; Lafon, O.; Trébosc, J.; Duk Kim, K.; Stampfl, C.; Baiker, A.; Amoureux, J.-P.; Huang, J. Brønsted acid sites based on penta-coordinated aluminum species. *Nat. Commun.* **2016**, *7*, 13820.
(31) Kerber, R. N.; Kermagoret, A.; Callens, E.; Florian, P.; Massiot, D.; Lesage, A.; Copéret, C.; Delbecq, F.; Rozanska, X.; Sautet, P. Nature and Structure of Aluminum Surface Sites Grafted on Silica from a Combination of High-Field Aluminum-27 Solid-State NMR Spectroscopy and First-Principles Calculations. *J. Am. Chem. Soc.* **2012**, *134* (15), 6767−6775.
(32) Lam, E.; Comas-Vives, A.; Copéret, C. Role of Coordination Number, Geometry, and Local Disorder on 27Al NMR Chemical Shifts and Quadrupolar Coupling Constants: Case Study with Aluminosilicates. *J. Phys. Chem. C* **2017**, *121* (36), 19946−19957.
(33) Wischert, R.; Florian, P.; Copéret, C.; Massiot, D.; Sautet, P. Visibility of Al Surface Sites of γ-Alumina: A Combined Computational and Experimental Point of View. *J. Phys. Chem. C* **2014**, *118* (28), 15292−15299.
(34) Engelhardt, G.; Michel, D. *High-Resolution Solid-State NMR of Silicates and Zeolites*, Wiley & Sons Austria, Limited: United States, 1987.
(35) Hunger, M. Multinuclear solid-state NMR studies of acidic and non-acidic hydroxyl protons in zeolites. *Solid State Nucl. Magn. Reson.* **1996**, *6* (1), 1−29.
(36) Frydman, L.; Harwood, J. S. Isotropic Spectra of Half-Integer Quadrupolar Spins from Bidimensional Magic-Angle Spinning NMR. *J. Am. Chem. Soc.* **1995**, *117* (19), 5367−5368.
(37) Han, O. H.; Kim, C.-S.; Hong, S. B. Direct Evidence for the Nonrandom Nature of Al Substitution in Zeolite ZSM-5: An Investigation by 27Al MAS and MQ MAS NMR. *Angew. Chem., Int. Ed.* **2002**, *41* (3), 469−472.
(38) Jiao, J.; Kanellopoulos, J.; Wang, W.; Ray, S. S.; Foerster, H.; Freude, D.; Hunger, M. Characterization of framework and extra-framework aluminum species in non-hydrated zeolites Y by 27Al spin-echo, high-speed MAS, and MQMAS NMR spectroscopy at B_0 = 9.4 to 17.6 T. *Phys. Chem. Chem. Phys.* **2005**, *7* (17), 3221−3226.
(39) Almutairi, S. M.; Mezari, B.; Filonenko, G. A.; Magusin, P. C. M.; Rigutto, M. S.; Pidko, E.; Hensen, E. J. M. Influence of Extraframework Aluminum on the Bronsted Acidity and Catalytic Reactivity of Faujasite Zeolite. *ChemCatChem* **2013**, *5*, 452−466.
(40) Abdolrahmani, M.; Chen, K.; White, J. L. Assessment, Control, and Impact of Brønsted Acid Site Heterogeneity in Zeolite HZSM-5. *J. Phys. Chem. C* **2018**, *122* (27), 15520−15528.
(41) Nystrom, S.; Hoffman, A.; Hibbitts, D. Tuning Brønsted Acid Strength by Altering Site Proximity in CHA Framework Zeolites. *ACS Catal.* **2018**, *8*, 7842−7860.
(42) Li, S.; Zheng, A.; Su, Y.; Zhang, H.; Chen, L.; Yang, J.; Ye, C.; Deng, F. Brønsted/Lewis Acid Synergy in Dealuminated HY Zeolite: A Combined Solid-State NMR and Theoretical Calculation Study. *J. Am. Chem. Soc.* **2007**, *129* (36), 11161−11171.
(43) Fritz, P. O.; Lunsford, J. H. The effect of sodium poisoning on dealuminated Y-type zeolites. *J. Catal.* **1989**, *118* (1), 85−98.
(44) Mota, C. J. A.; Bhering, D. L.; Rosenbach, N. A DFT Study of the Acidity of Ultrastable Y Zeolite: Where Is the Brønsted/Lewis Acid Synergism? *Angew. Chem., Int. Ed.* **2004**, *43* (23), 3050−3053.
(45) Bhering, D. L.; Ramírez-Solís, A.; Mota, C. J. A. A Density Functional Theory Based Approach to Extraframework Aluminum Species in Zeolites. *J. Phys. Chem. B* **2003**, *107* (18), 4342−4347.
(46) Ernst, H.; Freude, D.; Wolf, I. Multinuclear solid-state NMR studies of Brønsted sites in zeolites. *Chem. Phys. Lett.* **1993**, *212* (6), 588−596.
(47) Fyfe, C. A.; Betherton, J. L.; Lam, L. Y. Solid-State NMR Detection, Characterization, and Quantification of the Multiple Aluminum Environments in USY Catalysts by ^{27}Al MAS and MQMAS Experiments. *J. Am. Chem. Soc.* **2001**, *123*, 5285−5291.
(48) Chen, K.; Gumidyala, A.; Abdolrhamani, M.; Villines, C.; Crossley, S.; White, J. L. Trace water amounts can increase benzene H/D exchange rates in an acidic zeolite. *J. Catal.* **2017**, *351*, 130−135.
(49) Silaghi, M.-C.; Chizallet, C.; Sauer, J.; Raybaud, P. Dealumination mechanisms of zeolites and extra-framework aluminum confinement. *J. Catal.* **2016**, *339* (Supplement C), 242−255.
(50) Stanciakova, K.; Ensing, B.; Göltl, F.; Bulo, R. E.; Weckhuysen, B. M. Cooperative Role of Water Molecules during the Initial Stage of Water-Induced Zeolite Dealumination. *ACS Catal.* **2019**, *9* (6), 5119−5135.
(51) Pickard, C. J.; Mauri, F. All-electron magnetic response with pseudopotentials: NMR chemical shifts. *Phys. Rev. B: Condens. Matter Mater. Phys.* **2001**, *63* (24), 245101.
(52) Petrilli, H. M.; Blöchl, P. E.; Blaha, P.; Schwarz, K. Electric-field-gradient calculations using the projector augmented wave method. *Phys. Rev. B: Condens. Matter Mater. Phys.* **1998**, *57* (23), 14690−14697.

https://dx.doi.org/10.1021/jacs.0c00590
J. Am. Chem. Soc. 2020, 142, 7514−7523

(53) Babitz, S. M.; Williams, B. A.; Miller, J. T.; Snurr, R.; Haag, W.; Kung, H. H. Monomolecular cracking of n-hexane on Y, MOR, and ZSM-5 zeolites. *Appl. Catal., A* **1999**, *179*, 71−86.
(54) Ravi, M.; Sushkevich, V. L.; van Bokhoven, J. A. Lewis Acidity Inherent to the Framework of Zeolite Mordenite. *J. Phys. Chem. C* **2019**, *123* (24), 15139−15144.
(55) van Bokhoven, J. A.; Koningsberger, D. C.; Kunkeler, P.; van Bekkum, H.; Kentgens, A. P. M. Stepwise Dealumination of Zeolite Beta at Specific T-Sites Observed with 27Al MAS and 27Al MQ MAS NMR. *J. Am. Chem. Soc.* **2000**, *122* (51), 12842−12847.
(56) van Bokhoven, J. A.; Roest, A. L.; Koningsberger, D. C.; Miller, J. T.; Nachtegaal, G. H.; Kentgens, A. P. M. Changes in Structural and Electronic Properties of the Zeolite Framework Induced by Extraframework Al and La in H-USY and La(x)NaY: A 29Si and 27Al MAS NMR and 27Al MQ MAS NMR Study. *J. Phys. Chem. B* **2000**, *104* (29), 6743−6754.
(57) van Bokhoven, J. A.; van der Eerden, A. M. J.; Koningsberger, D. C. Three-Coordinate Aluminum in Zeolites Observed with In situ X-ray Absorption Near-Edge Spectroscopy at the Al K-Edge: Flexibility of Aluminum Coordinations in Zeolites. *J. Am. Chem. Soc.* **2003**, *125* (24), 7435−7442.
(58) Janda, J.; Bell, A. T. Effects of Si/Al Ratio on the Distribution of Framework Al and on the Rates of Alkane Monomolecular Cracking and Dehydrogenation in H-MFI. *J. Am. Chem. Soc.* **2013**, *135*, 19193−19207.
(59) Yang, C.; Janda, A.; Bell, A. T.; Lin, L. Atomistic Investigations of the Effects of Si/Al Ratio and Al Distribution on the Adsorption Selectivity of n-Alkanes in Brønsted-Acid Zeolites. *J. Phys. Chem. C* **2018**, *122*, 9397−9410.
(60) Gounder, R.; Iglesia, E. The Catalytic Diversity of Zeolites: Confinement and Solvation Effects within Voids of Molecular Dimensions. *Chem. Commun.* **2013**, *49*, 3491−3509.
(61) Gorte, R. J.; Crossley, S. P. A Perspective on Catalysis in Solid Acids. *J. Catal.* **2019**, *375*, 524−530.
(62) Crossley, S. P.; Resasco, D. E.; Haller, G. L. Clarifying the Multiple Roles of Confinement in Zeolites: From stabilization of transition states to modification of internal diffusion rates. *J. Catal.* **2019**, *372*, 382−387.
(63) To, A. T.; Jentoft, R.; Alvarez, W. E.; Crossley, S. P.; Resasco, D. E. Generation of Synergistic Sites by Thermal Treatment of HY Zeolite. Evidence from the Reaction of Hexane Isomers. *J. Catal.* **2014**, *317*, 11−21.
(64) Zhang, Y.; Zhao, R.; Sanchez-Sanchez, M.; Haller, G. L.; Hu, J.; Bermejo-Deval, R.; Liu, Y.; Lercher, J. A. Promotion of Protolytic Pentane Conversion on H-MFI Zeolite by Proximity of Extra-framework Aluminum Oxide and Bronsted Acid Sites. *J. Catal.* **2019**, *370*, 424−433.

https://dx.doi.org/10.1021/jacs.0c00590
J. Am. Chem. Soc. 2020, 142, 7514−7523